

Cite this: *Energy Environ. Sci.*,
2019, 12, 756

Flexible GaAs solar cells on roll-to-roll processed epitaxial Ge films on metal foils: a route towards low-cost and high-performance III–V photovoltaics†

P. Dutta,^{id}*^{abc} M. Rathj,^{id}^{abc} D. Khatiwada,^{abc} S. Sun,^{abc} Y. Yao,^{abc} B. Yu,^{abc}
S. Reed,^a M. Kacharia,^d J. Martinez,^e A. P. Litvinchuk,^c Z. Pasala,^f S. Pouladi,^a
B. Eslami,^a J.-H. Ryou,^{id}^{abc} H. Ghasemi,^{id}^a P. Ahrenkiel,^f S. Hubbard^d and
V. Selvamanickam^{abc}

In this report, we describe a unique roll-to-roll plasma-enhanced chemical vapor deposition (R2R-PECVD) technique to grow high-quality single-crystalline-like Ge films on flexible metal foils, an important advancement towards scalable processing of epitaxial Ge films at low-cost. Ion-beam assisted deposition was used to create single-crystalline-like substrate templates to enable epitaxial growth of Ge films. The Ge films were highly (004) oriented, biaxially-textured and showed remarkable crystalline quality, equivalent to single-crystal Ge wafers. Subsequently, the Ge films on metal foils were used as substrates to fabricate flexible GaAs single-junction solar cell by metal-oxide chemical vapor deposition (MOCVD). The champion device showed efficiency of 11.5%, and the average efficiency of four devices was 8% at 1 sun, the highest reported on GaAs PV directly deposited on alternative flexible substrates. Devices made on CVD-Ge film exhibited significantly improved performance compared to the ones grown on sputtered Ge films. Scalable production of inexpensive and flexible epi-Ge films will not only be useful for developing low-cost and high-performance III–V solar cells, but also for emerging flexible electronic devices applications.

Received 3rd September 2018,
Accepted 18th January 2019

DOI: 10.1039/c8ee02553c

rsc.li/ees

Broader context

While contribution of solar energy to the overall energy mix is increasing at a rapid pace, drastically-new technologies are needed for it to be competitive with fossil fuels on a global scale. Gallium arsenide-based photovoltaics with its demonstrated efficiency values nearly twice as high as that of widely-used polycrystalline silicon solar cells are an obvious choice. But, their high cost, primarily due to high cost of wafers, has been an impediment. If GaAs-based photovoltaics can be fabricated on inexpensive metal substrates by continuous roll-to-roll manufacturing, there is an opportunity to combine high efficiencies with low cost. In this publication, we demonstrate a unique roll-to-roll plasma-enhanced chemical vapor deposition (R2R-PECVD) technique to grow high-quality single-crystalline-like Ge films even on flexible metal substrates. These substrates have been used to fabricate flexible GaAs single-junction solar cells by metal-oxide chemical vapor deposition (MOCVD) with conversion efficiency as high as 11.5%. GaAs-based solar cells fabricated by direct deposition on metal foils by roll-to-roll processing could be a breakthrough needed for solar energy to be competitive with fossil fuels. Additionally, the flexible, epitaxial Ge and GaAs films demonstrated in this work can be impactful for flexible electronics too.

^a Department of Mechanical Engineering, University of Houston, Houston, TX 77204, USA. E-mail: pdutta2@uh.edu

^b Advanced Manufacturing Institute, University of Houston, Houston, TX 77204, USA

^c Texas Center for Superconductivity, University of Houston, Houston, TX 77204, USA

^d Department of Physics & Microsystems Engineering, Rochester Institute of Technology, Rochester, NY 14623, USA

^e Materials Evaluation Laboratory, NASA Johnson Space Center, Houston, TX 77085, USA

^f Nanoscience and Nanoengineering, South Dakota School of Mines and Technology, Rapid City, SD 57701, USA

† Electronic supplementary information (ESI) available. See DOI: 10.1039/c8ee02553c

1. Introduction

III–V compound semiconductor solar cells have achieved the highest photo-conversion efficiency so far with single-junction GaAs and multijunction III–V solar cells demonstrating efficiencies of over 28 and 35% respectively at 1 sun.¹ Ideal direct band-gap, long-term stability, radiation hardness and excellent opto-electronic properties of GaAs and related III–V compounds are highly suitable for high-efficiency photovoltaics (PV). However, the high-cost of III–V PV has prevented the large-scale

Table 1 Single-junction (SJ) GaAs solar cell efficiencies on reusable and alternative substrates measured under the global AM 1.5 spectrum

Type	Technique	Substrate	Efficiency (%)	Ref.
SJ GaAs (f)	Epitaxial lift off (ELO)	Reusable GaAs wafer	28.8	Kayes <i>et al.</i> ⁷
SJ GaAs (r)	SiGe grading	Silicon wafer	18.1	Andre <i>et al.</i> ¹⁴
SJ GaAs (r)	Selective area growth	Patterned Si wafer	10.4	Vaisman <i>et al.</i> ²¹
SJ GaAs (r)	Mechanical Bonding	Silicon wafer	13.25	Kim <i>et al.</i> ⁸
SJ poly-GaAs (r)	Direct growth	Poly-Ge wafers	18.2	22 and 23
SJ poly-GaAs (f)	Direct growth	Poly-Ge on Mo foil	9.2	24 and 25
SJ SCL-GaAs (f)	Direct growth/seed-and-epitaxy (IBAD)	SCL-Ge template on Hastelloy metal foil	11.5	This work

f – flexible r – rigid SCL = single-crystalline-like

adoption in mainstream terrestrial market and limited their use to only niche applications, primarily in space PV. It is widely accepted that the material and manufacturing costs need to be substantially reduced in order to make III–V PV viable for commercial market.

Efforts have been made over several decades to find alternative cost-effective techniques to manufacture III–V PV. Table 1 provides the efficiencies of single-junction GaAs solar cell (measured at AM 1.5) fabricated on reusable GaAs and alternative substrates. One of the major costs originates from the expensive Ge and GaAs single-crystal wafers, which are used as substrates to epitaxially grow the III–V PV devices. To address this, epitaxial lift-off (ELO) and transfer techniques were developed, and III–V solar cells were fabricated.^{2–6} Record efficiency of above 28% was achieved in SJ GaAs solar cells using this method.⁷ In these processes, III–V devices were lifted-off from the parent wafer and transferred to low-cost substrates, allowing multiple reuse of the parent wafer. Another III–V and low-cost substrate integration approach use mechanical bonding.⁸ However, the process scalability and cost benefits of reusing the wafers using the lift-off and bonding techniques are still unclear. It is evident from the present low-market share of III–V PV that these wafer reuse and transfer printing techniques have not been effective enough to render the III–V PV cost-competitive with Si, CdTe, CIGS and other existing PV technologies.^{9,10} It is imperative that a true scalable process of producing the III–V solar cells needs to be developed to further lower down the costs.

Another alternative approach is to directly grow III–V PV and compound semiconductors on non-epitaxial low-cost substrates. Replacement of the epi-Ge and GaAs wafers with inexpensive substrates was expected to substantially reduce the cost of the devices. However, the challenge was to identify a low-cost substrate which has lattice/thermal match with GaAs and that can sustain the high growth temperatures. Hetero-epitaxial GaAs growth was demonstrated on bulk single-crystal Si wafers (4% lattice mismatch, low-cost) using SiGe composition grading, thermal cycling and thick buffer layers (> 3 μm) to account for the lattice mis-match of GaAs and Si and suppress misfit defects.^{11–13} Highest efficiency of 18.1% was achieved in single-junction GaAs solar cells on Si substrate with TDD of $1.8 \pm 0.2 \times 10^6 \text{ cm}^{-2}$.¹⁴ However, the efficiency of the GaAs/Si devices was limited due to the challenges in achieving low threading dislocation density ($< 10^6 \text{ cm}^{-2}$).^{15–17} Moreover, use

of thick buffer layers added to the cost of the device, rendering them cost prohibitive for commercial applications. Selective-area growth (SAG) is another alternative technique to achieve high-quality GaAs on low-cost nano-patterned substrates without the use of thick buffer layers.^{18–20} Single-junction GaAs solar cells of 10.4% efficiency were fabricated on inactive V-grooved Si substrates using the SAG method.²¹ In another approach, GaAs films were deposited on poly-Ge wafers (with sub mm grains) and the devices demonstrated moderate efficiencies, but the cost-benefit was minimal.^{22,23} Furthermore, GaAs solar cell on large-grained re-crystallized Ge films on Mo and W/graphite substrates yielded poly-crystalline GaAs devices with efficiency of ~10%.^{24,25} In general, direct growth of GaAs on poly-crystalline substrates resulted in polycrystalline GaAs films with μm mm sized grains with large-angle grain boundaries, intragrain and grain boundary defects, which acted as carrier recombination centers and deleteriously affected the device performance.²⁶ Challenges in achieving PV quality poly-GaAs on alternative substrates stunted the progress of the poly-GaAs technology over the last decade.

To achieve higher-quality ordered (single-crystal-like) films on non-epitaxial alternative substrates, “seed-and-epitaxy” approaches have been developed where thin seed layers with good crystalline order were used as a template for subsequent epitaxial growth of the PV absorber.²⁷ Single-crystal-like biaxially-textured Ge films were obtained on polycrystalline metal and amorphous glass substrates using ion-beam assisted deposition (IBAD) or oblique-angle deposition technique.^{28–32} IBAD is a process by which a biaxially-textured film (a film aligned both in-plane and out-of-plane directions) can be achieved on essentially any substrate at room temperature, using simultaneous deposition (sputter, e-beam evaporation, *etc.*) and low-energy ion-assist (typically argon) at a certain incident angle.³⁶ As opposed to a polycrystalline film where grains are highly misoriented (> 10 degrees misorientation angle) and disordered, a biaxially-textured film consists of crystalline grains which are aligned to each other both in the in-plane and out-of-plane directions, assuming a single-crystalline-like structure with grain misorientation angle less than 5 degrees. Similar IBAD technique was employed to grow epi-Si films, Si solar cells and GaN LEDs on flexible metal substrates and is also routinely used in the high-temperature superconductor (HTS) wire industry.^{33–36} The biaxially-textured films were highly aligned both in the in-plane and out of-plane directions and the grain-boundary angles were

significantly lower compared to polycrystalline films.³⁶ In another method, biaxially-textured Ge (111) and Ge (00 l) were obtained on rolled cube-textured NiW (200) substrates using CaF₂ (111) and CeO₂ (00 l) as intermediate layers respectively employing rolling-assisted biaxially-textured substrates (RABiTS) technique.³⁷ a well-established commercial method to develop biaxially-textured metal substrates for epitaxial growth of high temperature superconductor films. It was noted that substantially better crystallographic alignment was achieved in (002) Ge templates compared to the (111) Ge templates. The high-alignment of the grains and low-angle-grain boundaries of biaxially-textured films were expected to be less detrimental to the device properties, leading to higher efficiencies. We have previously demonstrated epitaxial growth of single-crystalline-like GaAs films on low-cost, lightweight flexible metal foils using Ge films based on IBAD templates.^{38,39} Single-crystal-like Ge film templates, grown by roll-to-roll sputter deposition on IBAD textured buffers on metal foils, were used as substrates for epi-GaAs growth.^{39,40} The GaAs films consisted of 2–4 μm grains with (00 l) orientation, strong biaxial texture and ultra-low-angle grain boundaries (<1 degree) and exhibited strong photoluminescence, carrier lifetime of ~ 2 ns and high carrier mobilities, all indicating promise for high-performance PV application.^{38,39} However, to further improve the quality of the sputtered Ge template and to enable higher quality GaAs films, it was essential to develop a roll-to-roll process for Ge deposition using chemical vapor deposition method, a process which is known to yield device-quality semiconductor films and popularly used in the industry.

In this paper, we demonstrate for the first time, a method to directly grow epi-Ge films on flexible and inexpensive metal substrates using roll-to-roll (R2R) plasma-enhanced chemical vapor deposition (PECVD). The ability to continuously deposit epi-Ge films by R2R CVD process was expected to improve both the Ge film quality (as opposed to sputtered Ge films) and process scalability. IBAD based “seed-and-epitaxy” method was used to obtain the epitaxy-enabling buffer template needed for epi-Ge growth.⁴⁰ In addition, we also demonstrate epitaxial GaAs growth by metal-organic chemical vapor deposition (MOCVD) and a proof-of-concept single-junction GaAs solar cell on the epi-Ge templates. The properties of R2R processed epi-Ge films and relative improvement with respect to the underlying sputtered Ge template have been described in detail. Furthermore, we have provided an in-depth insight on the properties of the epi-GaAs films and the design and fabrication of the flexible GaAs solar cell on metal substrates. The device current-voltage properties and quantum efficiency were also investigated.

2. Fabrication scheme

I. Development of epitaxial buffer layers on metal: seed and epitaxy by IBAD

To achieve GaAs epitaxy on non-epitaxial metal substrates, we adopted the seed-and-epitaxy approach using the IBAD technique to develop an appropriate lattice, thermal and structurally-matched

buffer template which enables GaAs epitaxy. The IBAD technique can be used to produce a highly-aligned single-crystal-like film on an amorphous or polycrystalline substrate at room temperature.^{35,36} The fabrication of the multilayered buffer stack is by R2R thin film deposition processes whose details are described elsewhere.^{32,39,40} Briefly, the process began with 50 μm thick, 1.2 cm wide electropolished C-276 Hastelloy metal foils (Fig. 1 (a)), which are high-temperature tolerant and mechanically robust, amenable to growths at elevated temperatures. All the subsequent oxide buffer layers were deposited by continuous R2R PVD processes and meter lengths of the films were obtained at each layer.^{32,40} The multi-layered oxide buffer is shown in Fig. 1(b). First, an 80 nm Al₂O₃ layer was deposited by reactive RF sputtering which served as the diffusion barrier preventing metallic element diffusion from the substrate to the upper layers. Next, a thin 5 nm Y₂O₃ layer was deposited by ion beam sputtering which served as a nucleation layer for the IBAD MgO layer. Subsequently, a MgO layer (10 nm thick) was deposited using IBAD process at room temperature which resulted in single-crystal-like highly (002) oriented MgO films, providing the platform for heteroepitaxy of the subsequent layers.^{33,40} The alignment occurs within 10 nm of MgO thickness during the rapid roll-to-roll process. Next, a 60 nm thick epi-MgO layer was grown by reactive sputtering at higher temperature (~ 500 °C) on the IBAD MgO layer to improve the crystalline quality. To enable Ge epitaxy, intermediate LaMnO₃ (50 nm) and CeO₂ (200 nm) layers were deposited by magnetron sputtering to match the lattice and structure of Ge.⁴⁰ The CeO₂ layer (cubic-fluorite), with a good structural match with Ge (cubic-diamond, $\sim 4\%$ mismatch) enabled epitaxial growth of Ge. A photograph of a CeO₂ buffer segment is shown in Fig. 1(b). Next, Ge layer was deposited by R2R radio-frequency (RF) sputtering on the CeO₂ buffer layer resulting in single-crystal-like epi-Ge films with (004) orientation and strong biaxial texture, as shown in Fig. 1(c).^{32,40} The sputtered epi-Ge films on metal foils have been previously used as substrates for GaAs growth.^{38,39} However, high density of defects in the sputtered epi-Ge layer led to equivalent high-level of defect density in the GaAs films, deleteriously affecting the quality and performance of the devices. Therefore, improvement of the Ge layer was necessary to achieve device-quality epi-GaAs films.

II. Roll-to-roll PECVD of epi-Ge on metal foil

To further improve the quality of the sputtered Ge layer, a PECVD Ge layer was coated over the sputtered Ge layer. A photograph of a segment of epi-Ge CVD film on sputtered Ge template on metal foil is shown in Fig. 1(c). CVD thin films, deposited in equilibrium with high purity precursors, are known to yield substantially high-quality (device-quality) material compared to sputtered films. A custom-designed R2R CVD chamber was developed to enable continuous growth of semiconductor films on flexible substrates. A schematic of the R2R chamber is shown in Fig. 2(a). The chamber was fitted with IR lamps which can heat up-to 1300 °C. Germane (GeH₄) with 99.999 purity and hydrogen, purified by a palladium cell to ppb level, were used as process gases at a pressure of 2 Torr and

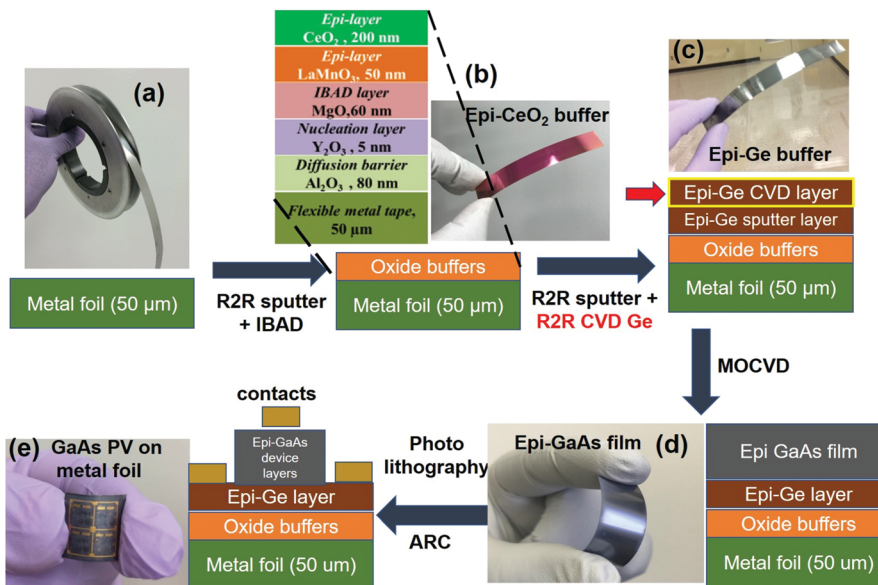


Fig. 1 (a) Photograph of Hastelloy C-276 metal foil rolled in a spool used as starting substrate for roll-to-roll depositions. (b) Photograph and schematic of CeO_2 epitaxial buffer on metal foil using buffer layers grown by ion-beam assisted deposition and sputtering. Magnified image shows the multi-layered architecture of epitaxial buffer layers underneath CeO_2 layer. (c) Photograph and schematic of epitaxial single-crystalline-like Ge layer deposited by roll-to-roll CVD and sputter deposition on the metal foil. The epi-Ge layer made by CVD process is shown by the red arrow. (d) Photograph of a segment and schematic of epi-GaAs thin film deposited on CVD-Ge template by MOCVD. (e) Schematic of a fabricated single-junction GaAs solar cell on CVD-Ge template on metal foil and a photograph of a flexible SJ solar GaAs solar cell.

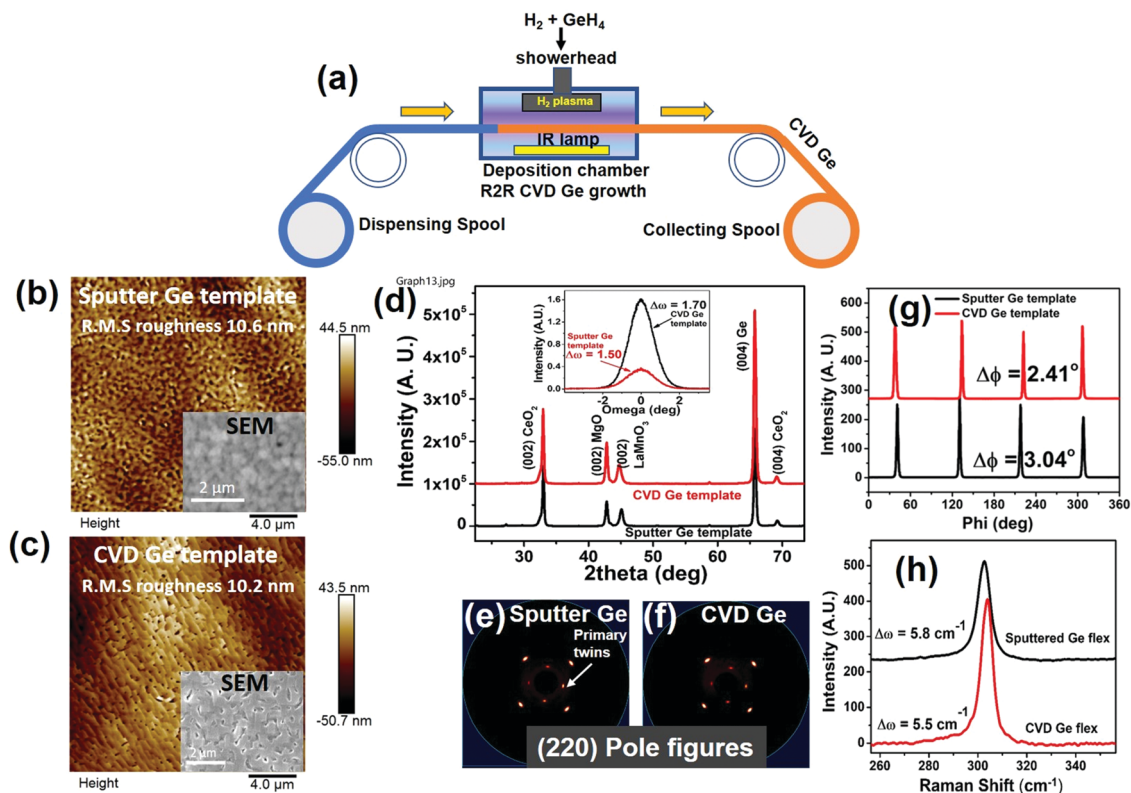


Fig. 2 (a) Schematic of roll-to-roll PECVD Ge deposition chamber enabling continuous growth of epitaxial Ge films on metal foils. (b) AFM surface morphology of sputtered Ge template; inset shows corresponding SEM surface morphology. (c) AFM surface morphology of CVD Ge template; an inset shows corresponding SEM surface morphology. (d) XRD theta–2theta scans of CVD and sputtered Ge templates and corresponding rocking curves in the inset. (e) and (f) show the (220) pole figures of sputtered and CVD Ge template respectively. (g) XRD Phi scans of sputtered and CVD Ge templates showing four fold symmetry. (h) Raman spectra of sputtered and CVD Ge templates on metal foils.

temperature of 650 °C. A radio-frequency inductively-coupled (ICP) H₂ plasma of 250 W was used during the CVD Ge growth which substantially improved the growth rate and precursor utilization. A tape moving speed of 6 cm min⁻¹ was used to achieve a thickness of ~ 1 μm in the Ge films. Long lengths of CVD epi-Ge films on metal foils were obtained which were subsequently used for GaAs growth. This is one of the very first reports of PECVD growth of epitaxial Ge films on flexible substrates by continuous R2R process, which is highly promising for high-volume scalable manufacturing of epi-Ge films at low-cost on alternative substrates.

III. GaAs MOCVD and device fabrication

III–V thin films were grown on CVD Ge template using a custom-built MOCVD tool with dual chambers.^{38,39} Segments of CVD Ge films were used as substrates for GaAs growth. Photograph of a GaAs film on CVD Ge template on metal foil is shown in Fig. 1(d), along with the schematic of the layer architecture. A custom-designed graphite susceptor was employed to hold the flexible substrates to ensure uniform heating of the samples in the MOCVD reactor. Trimethyl gallium (TMGa), trimethyl aluminum (TMAI) and arsine (AsH₃) were used as Ga, Al and As sources, respectively. Silane (SiH₄) and diethyl zinc (DEZn) were used as an n-type and p-type dopant respectively due to their low memory effect. H₂, highly purified by a palladium cell to ppb levels, was used as the carrier gas. The chamber pressure was fixed at 20 Torr. While the GaAs films were grown at an optimized temperature of 650 °C, AlGaAs films were deposited at an elevated temperature of 750 °C.⁴¹ The device fabrication started with the deposition of undoped intrinsic GaAs layer of ~2 μm thick on CVD Ge template on metal foil. Previously, it was observed that Ge diffuses about 500 nm in the GaAs layer and defect density decreases significantly with thickening of the GaAs layer.⁴² Thus, the role of this undoped GaAs layer was to act as a Ge diffusion barrier and to reduce defect density of the GaAs layer prior to deposition of the p–n junction. Next, a highly doped p++ GaAs layer of bulk carrier concentration (B.C.) 1 × 10¹⁹ cm⁻³ and 1.5 μm thickness was deposited to create a lateral current conduction layer for side contacts. Due to the intermediate oxide buffer, back contacts were not possible in the devices. Subsequently, 30 nm p++ AlGaAs layer back-surface field (B.C. = 1 × 10¹⁹ cm⁻³), 1.2 μm p-GaAs base (B.C. = 1 × 10¹⁷ cm⁻³), 50 nm n+ GaAs emitter (B.C. = 5 × 10¹⁸ cm⁻³), 20 nm n++ AlGaAs window layer (B.C. = 1 × 10¹⁹ cm⁻³) and 30 nm n++ GaAs cap layer (B.C. = 1 × 10¹⁹ cm⁻³) were deposited. A schematic and photograph of a fabricated GaAs solar cell on metal substrate are shown in Fig. 1(e).

Devices were fabricated using the photolithography technique, which included mesa formation to isolate the cells, deposition of top contact of Au/Ge/Ni (200/10/5 nm) and bottom contacts of Au/Zn (200/15 nm) by e-beam evaporation for n-GaAs and p-GaAs respectively and pattern formation using metal lift-off process. Transfer length measurement (TLM) was performed by deposition of metal pads with different separations to determine the sheet and contact resistance of the top and bottom contacts. The contact resistances were 5.5 and

3 Ohms for the top and bottom contact respectively. Achieving appropriate flatness of the sample surface during the photolithography steps was essential to obtain the desired pattern resolution and device yield. Etching of the flexible GaAs was performed using sulphuric acid (H₂SO₄):hydrogen peroxide (H₂O₂):distilled water (H₂O) solution in 1:8:280 ratio which resulted in etch rate of ~120 nm min⁻¹. Removal of the parasitic absorption layer (cap layer) was performed using the same etch solution leading to an increase in the photocurrent. Finally, a double layer anti-reflection coating (ARC) of zinc sulfide (48 nm) and magnesium fluoride (102 nm) was deposited using e-beam evaporation which further enhanced the photon absorption and current density of the solar cells.

High resolution transmission electron microscopy (TEM) plan-view imaging was carried out using a JEM-2100 LaB6 microscope at 200 keV. Several locations (at least 5 spots) of representative samples (>4) were imaged to obtain a reliable defect density count. In order to study the crystallographic orientation and microstructural quality of the epilayers, high resolution X-ray diffraction (HRXRD) theta-2theta and rocking curve scans were conducted using a triple-axis Bruker D8 diffractometer. X-ray pole figure measurements were conducted using a Bruker 2D General Area Detector Diffraction System. Phi scans extracted from the pole figures were used to determine in-plane texture of the films. Scanning Electron Microscopy (SEM) imaging was carried out in a 55VP Zeiss SEM at 20 kV in variable pressure (VP) mode using a current of 10 × 10¹⁵ nA. Raman spectra were acquired with a triple T64000 spectrometer (Horiba) employing a blue 488 nm excitation laser wavelength in the backscattering geometry, using 50× objective to focus the incident laser beam and to collect scattered radiation. The laser intensity was kept low (<3 mW) to prevent laser-induced modification of the Si surface. Hall measurements were conducted in Van der Pauw geometry using a HMS-5000 Ecopia system at room temperature. The carrier mobility was measured on several segments of the flexible Ge samples across a 50 cm length and an average value and standard deviation were reported.

3. Results and discussion

1. Properties of CVD Ge on flexible substrates

Fig. 2(b) and (c) show the AFM surface morphology (and the inset shows the SEM morphology) of the CVD Ge and sputter Ge thin film templates on metal substrates respectively. The surface of the CVD Ge film consisted of inter-connected grains with pit-like regions in between, different from the underlying sputtered Ge film which did not exhibit such structures. In addition, the CVD Ge film grains appeared to be more elongated compared to the underlying sputter Ge film. The CVD Ge films were marginally smoother (r.m.s. roughness ~ 9 ± 0.5 nm) compared to the underlying sputtered Ge layer (r.m.s. roughness ~ 10 ± 0.5 nm). It is to note here that without the hydrogen plasma assist, a much rougher and non-uniform film was obtained. A nominal thickness of ~1.1 ± 0.1 μm was achieved

in the CVD Ge template at the tape moving speed of 6 cm min^{-1} , as determined by focused ion beam cross-sections of multiple locations along the length of the films. The thickness of the sputtered Ge template was $\sim 800 \text{ nm}$, typically grown by the R2R sputter process.^{32,39,40} Fig. 2(d) shows the theta–2theta scan of the R2R Ge film and the underlying sputtered Ge substrate. Strong (004) peaks of Ge and absence of other orientations indicate a high degree of alignment towards the (00 l) direction. The inset shows rocking curves, comparing the CVD Ge and sputtered Ge films, with peak-widths of 1.49 and 1.70 degrees respectively. The decrease in peak-width in CVD Ge indicate improvement in crystalline quality compared to the underlying sputtered Ge. Fig. 2(e) and (f) show the XRD (220) pole figure of the sputtered and CVD Ge films respectively which reveal a strong four-fold symmetry, confirming strong biaxial texture in the film. Fig. 2(g) shows the phi scans of the sputtered and CVD Ge films, extracted from the pole figure maps. Average in-plane texture spreads, estimated by fitting the peaks using Gaussian function, are 2.41 and 3.04 degrees for CVD Ge and sputtered Ge respectively. Again, the narrower peak width of CVD Ge suggested higher in-plane alignment of grains. Next, the crystalline quality of the films was examined optically using Raman spectroscopy. Fig. 2(h) shows the Raman spectra of sputtered Ge and CVD Ge films. Both films exhibited an intense and narrow Raman peaks (transverse optical mode) at 302 cm^{-1} corresponding to crystalline Ge. No amorphous phase was observed. The Raman peak widths, determined using a Lorentzian fit of the peaks, were 5.8 and 5.5 cm^{-1} for sputtered and CVD Ge respectively. The narrower Raman peak-width of the CVD Ge film indicated improved crystallinity compared to the underlying sputtered Ge. Moreover, the peak-widths were significantly narrower (indicating better crystalline quality) compared to previously reported values of Ge films grown on c-Si and other alternative substrates.^{43,44} Finally, Hall mobility measurements were done at room temperature to

determine the carrier mobility. The unintentionally-doped CVD Ge films were n-type in character, with average carrier concentration of $\sim (2 \pm 0.5) \times 10^{18} \text{ cm}^{-3}$ and mobility of $230 \pm 20 \text{ cm}^2 \text{ V}^{-1} \text{ s}^{-1}$. In comparison, the sputtered Ge film exhibited a mobility of $80 \pm 20 \text{ cm}^2 \text{ V}^{-1} \text{ s}^{-1}$, substantially lower than that of the CVD-Ge film. It is evident from the results that coating the sputtered Ge layer with CVD Ge is important to improve the quality of the substrate and made it more conducive for high-quality GaAs growth. Furthermore, R2R continuous processing of CVD Ge helped in providing sufficient inventory of long lengths of Ge templates on metal foils for subsequent use as substrate for epi-GaAs deposition.

2. Properties of flexible GaAs on R2R CVD Ge

Fig. 3(a) and (b) shows the plan-view STEM image of undoped GaAs film deposited on CVD and sputtered Ge template respectively. Grain sizes of GaAs on sputtered and CVD Ge varied between $2\text{--}4 \mu\text{m}$.³⁸ It was clearly observed that the GaAs film on CVD Ge (Fig. 3a) exhibits far less defects (threading dislocations) compared to that on the sputtered Ge. Particularly, the inter-granular defects were substantially lower in the GaAs film on CVD Ge. Furthermore, while the defects spread across the GaAs film on the sputtered Ge template, majority of the defects in the GaAs film on CVD Ge were confined at the GB regions. The average threading dislocation density (TDD), counted manually employing several (>5) plan view images, was $4 \times 10^8 \text{ cm}^{-2}$ and $8 \times 10^8 \text{ cm}^{-2}$ for the GaAs films ($2 \mu\text{m}$ thick) on CVD Ge and sputtered Ge film respectively. The defect densities were significantly higher compared to those obtained in GaAs films on high-quality and low-defect density single-crystal Ge wafer substrates where TDDs were often not generated in high numbers due to the good lattice-match of GaAs and Ge. In our case, the defects were originated from the already highly-defective Ge template where TDDs were abundant due to the $>4\%$ lattice mismatch of Ge and

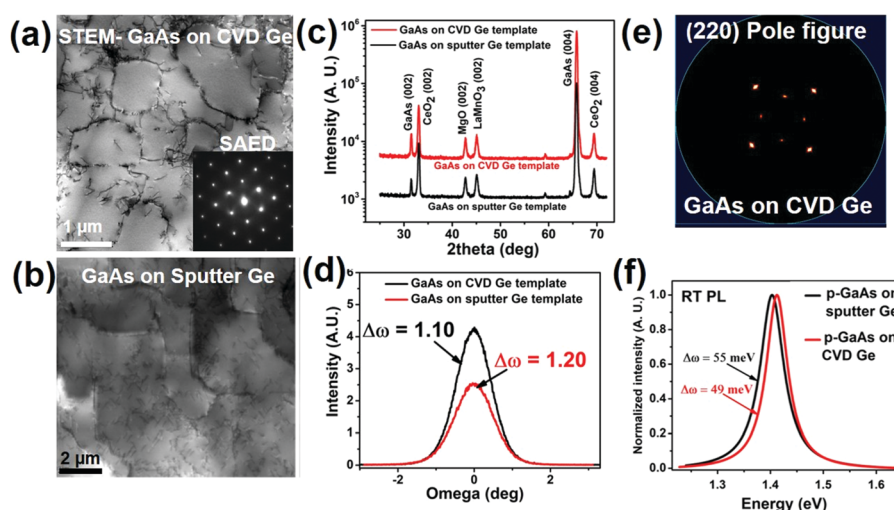


Fig. 3 (a) and (b) show STEM images of GaAs films deposited on CVD and sputtered Ge templates on meta foils. Inset of (a) shows the SAED pattern of GaAs film indicating single-crystalline nature of the GaAs film. (c) XRD theta–2theta scans of GaAs films deposited on CVD and sputtered Ge templates. (d) Rocking curves comparing the out-of-plane peak widths of GaAs films deposited on CVD and sputtered Ge templates. (e) Pole figure of GaAs film deposited on CVD Ge template. (f) RT PL spectra of GaAs films deposited on sputtered and CVD Ge templates.

CeO₂ buffer.^{38–40} Anti-phase defects (APDs) were also observed in the GaAs films due to growth on non-polar Ge templates. APDs are more common defects than TDDs during GaAs heteroepitaxy on Ge and are important to eliminate in order to achieve higher quality. However, the primary focus of this work was to control the TDDs and lower it using the CVD Ge films. At this point, no noticeable difference in APD density was observed in the GaAs films on sputtered and CVD Ge templates. A detailed analysis of the APDs in biaxially-textured GaAs films and their effect on film and device properties will be reported elsewhere. The selected-area electron diffraction pattern in the inset of Fig. 3(a) shows diffraction pattern corresponding to zinc blende structure, confirming single-crystalline nature of the film. Fig. 3(c) compares the XRD theta–2theta plot of GaAs grown on sputtered and CVD Ge templates. (004) and (002) peaks of zinc-blende GaAs verify the epitaxial growth with strong (00 l) orientation. “Out-of-plane peak widths ($\Delta\omega$), determined from the rocking curves, shown in the Fig. 3(d), are 1.10 and 1.20 degrees for GaAs on CVD Ge and sputtered Ge template respectively. The narrowing of $\Delta\omega$ from 1.49 degrees (CVD Ge template) to 1.10 degrees of GaAs on CVD Ge template, resulted in an improvement of texture and crystalline quality with GaAs deposition. Further, (220) pole figure of GaAs film on CVD Ge template, shown in Fig. 3(e), reveals a four-fold symmetry confirming strong biaxial texture. The in-plane texture ($\Delta\phi$) of GaAs film on CVD Ge template is 1.78 degrees as opposed to 2.2 degrees of GaAs on sputtered Ge template. Narrower $\Delta\omega$ and $\Delta\phi$ of GaAs film on CVD Ge template indicate a better crystalline quality compared to the GaAs film deposited on

sputtered Ge template. Results also indicated that improved grain alignment in CVD Ge films, as shown in the previous section, resulted in better alignment in the GaAs film on CVD Ge compared to that on the sputtered Ge counterpart.

Next, room temperature steady-state photoluminescence (PL) spectra were acquired to investigate the optical properties of the GaAs film. Fig. 3(f) shows the normalized PL spectra of p-doped GaAs films (carrier concentration of $1 \times 10^{18} \text{ cm}^{-3}$), deposited simultaneously on CVD and sputtered Ge templates. All the samples were measured under the same conditions using a fixed excitation wavelength (690 nm) and incident power (10 mW). Strong PL intensity corresponding to GaAs band-to-band transition was obtained, attesting to the high optical quality of the films. The peak locations were 1.42 and 1.415 eV, and the peak widths (full-width at half maxima obtained by fitting using Lorentz function) were 49 and 55 meV for GaAs film on CVD and sputtered Ge template respectively. In PL analysis, broadening of peak width and shifting of peak position from ideal band-gap transition energy (1.42 eV for GaAs) indicate lowering of film quality. Therefore, narrow peak-width and peak location coinciding with band-gap transition energy point to improved GaAs optical quality on CVD-Ge template compared to its sputtered-Ge counterpart, which can be attributed to the low-level of impurities and defects in the GaAs films on CVD-Ge template. Overall, the results clearly indicated the beneficial role of the CVD Ge layer in improving the optical and structural properties of the GaAs films.

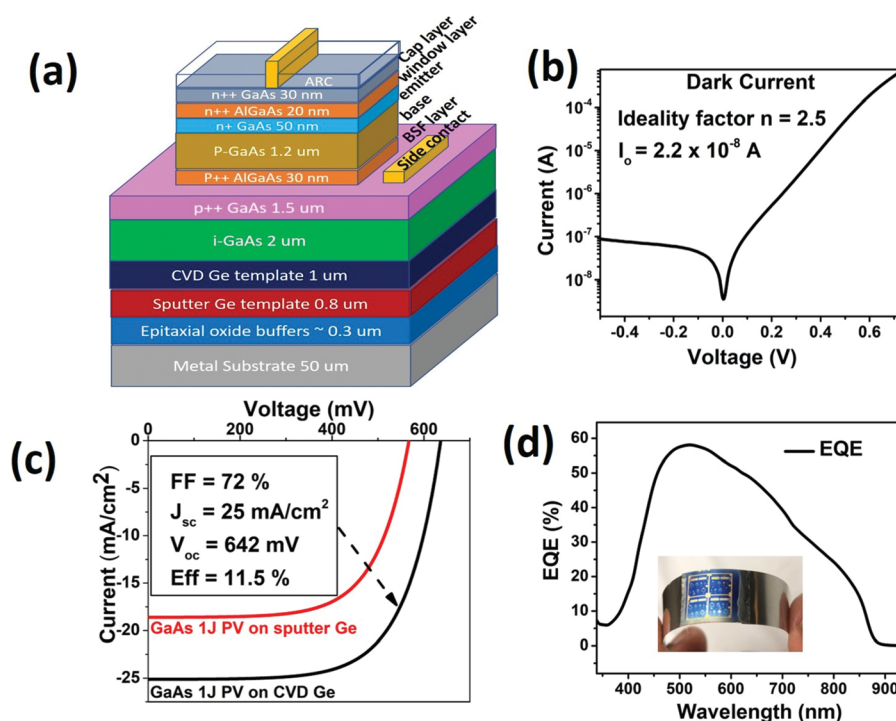


Fig. 4 (a) Schematic of the complete device architecture of the flexible GaAs solar cell made on metal foils (b) Dark I - V plot of single junction GaAs solar cell fabricated on CVD Ge template (c) Illuminated J - V plots of GaAs solar cells fabricated on CVD and sputtered Ge templates. (d) Representative EQE plot of a GaAs solar cell on CVD Ge template on metal foil. Inset shows the final fabricated flexible GaAs solar cell on metal foil substrates.

3. Flexible GaAs solar cell properties

Next, flexible single-junction (SJ) GaAs solar cells were fabricated on sputter and CVD Ge templates and their photovoltaic performance was investigated. Fig. 4(a) shows the detailed schematic of the architecture of the SJ GaAs solar cell on the CVD-Ge template. Solar cell with the same structure was deposited on sputter-Ge template (sans the CVD-Ge layer). Epi-AlGaAs window and BSF layers were developed and optimized separately on Ge-templates on metal substrate and incorporated here in the device structure.⁴¹ Device sizes of 500–1250 μm were fabricated, and the device properties were observed to be a function of the size. Devices of 500 μm diameter showed the best performance while the larger devices (750, 1000 and 1250 μm dia) showed a 10–15% drop in performance, which can be due to the increased number of grains and GBs in the device active area (see ESI† Table T3) Fig. 4(b) shows the dark-current *versus* voltage (I - V) plot for the flexible SJ GaAs solar cell (500 μm in diameter) on CVD-Ge template. Diode behavior with high rectification and distinct kick-in voltage was observed. The diode ideality factor (n) and reverse saturation current (I_0), determined by fitting the dark I - V curve using standard diode equation, were 2.6 (for voltages between 0.5 to 0.6 V) and 2.2×10^{-8} A respectively, which are higher than the previously reported n of ~ 2 and I_0 of $\sim 10^{-9}$ A for champion GaAs devices on wafer substrates.²⁶ The high value of n and I_0 of the flexible GaAs cell reported here suggest an increased non-radiative recombination which may be attributed to the high-density of grain boundaries, intra-grain defects and un-passivated sidewalls and perimeters of the flex-GaAs cells.⁴⁵ Currents flowing locally in the edge region, crystal defects and grain boundaries can also be a major contributing factor of non-ideal behavior and have been previously reported for Si and GaAs junctions with $n > 2$.²⁶ Efforts to improve the material quality (reduction of TDDs) as well as implementation of passivation techniques are currently underway to mitigate this recombination loss. InGaAs/GaAs strained SLs with two-step GaAs growth and combined thermal annealing steps led to a significant reduction in defect density by an order of magnitude. Further defect density reduction can be achieved by employing selected area epitaxy (SAE) which is currently in progress. In addition, hydrogen and phosphine plasma treatment as well as citric acid wet treatment are being carried out to passivate the GB and side-walls.⁴⁶ The impact of the GBs on film and device properties are currently under investigation and initial results suggest that the GBs at the p-n junction interface play an important role in the recombination characteristics of the devices.⁴⁷

Fig. 4(c) shows the illuminated current density *versus* voltage (J - V) plot of a SJ GaAs solar cell on CVD (black curve) and sputtered Ge (red curve) templates on metal substrates. An Oriel-200 solar simulator (calibrated by NREL) was used as the light source at 1 sun intensity (100 mW cm^{-2} , AM 1.5G) at 25 °C. The devices had the parasitic cap layer (30 nm highly doped GaAs layer) removed and an anti-reflection coating deposited to enhance light absorption. The top contacts created a 5% shadowing and the probe tips, which were placed directly on the top contacts during measurement, caused an additional

shadowing of 3% of the active area. The champion device showed efficiency of 11.5% at 1 sun. This is in good agreement with the modelling result reported by Jain *et al.* for GaAs with TDD of $\sim 10^8 \text{ cm}^{-2}$.⁴⁸ Short circuit current density (J_{sc}) of $25 \pm 0.4 \text{ mA cm}^{-2}$, open circuit voltage of $642 \pm 10 \text{ mV}$, and fill factor (FF) of $72 \pm 2\%$ were achieved in the champion cell after cap layer removal and with ARC coating. The initial as-fabricated, cap-layer removed, and ARC coated device parameters are shown in the ESI.† The average efficiency of multiple devices (>4) of same size fabricated in a batch was 8%. This is by far the highest efficiency achieved in GaAs SJ cells directly deposited on alternative flexible substrates. It is a substantial improvement from the 3.6% efficiency reported previously of GaAs SJ solar cell on poly-Ge on Mo substrate, and 1–2% efficiencies of Si solar cells on similar textured metal substrates.²⁴ Comparatively, the SJ GaAs solar cell fabricated on the sputtered Ge template showed a significantly reduced efficiency of 6.7% in the champion device, with J_{sc} of $18.6 \pm 0.4 \text{ mA cm}^{-2}$, V_{oc} of $570 \pm 10 \text{ mV}$ and FF of $63 \pm 3\%$. The average efficiency of 4 devices was 5%. The improved performance of the solar cells on CVD Ge templates may be attributed to higher quality of GaAs films on CVD Ge (lower defect density, higher crystalline quality and better alignment of the GaAs grains), as observed in the materials property investigation. Average series (R_s) and shunt resistances (R_{sh}) of both the devices, extracted from the slopes of the J - V curve near the short circuit current and open circuit voltage, were of 260 ± 50 and $1150 \pm 50 \text{ Ohms}$, respectively. In general, the devices were limited by low shunt resistance which may be due to the grain boundaries along the thickness of the cell causing shunt paths and also due to possible sidewall leakage. However, the series resistances were reasonably small which may be due to the low contact resistance of the top and bottom contacts. Also, there were no statistically significant differences in the devices made on CVD and sputtered Ge in terms of R_s and R_{sh} . The external quantum efficiency (EQE) of the SJ GaAs cell on metal substrate is shown in Fig. 4(d) was extracted from spectral response measured using an Oriel IQE-200 setup with a tungsten filament light source and Newport monochromator calibrated using Silicon and Germanium reference detectors. The quantum efficiency yield was moderate with a peak of $\sim 58\%$ at the lower wavelength region. The downward slope of QE from 500–800 nm suggest insufficient absorption in the base and/or short diffusion length of minority carriers. The EQE results were fitted to using the minority carrier drift-diffusion model, or Hovel model to extract diffusion lengths of $\sim 1.1 \mu\text{m}$ in the emitter and $\sim 0.2 \mu\text{m}$ in the base. We previously measured the carrier lifetime ($\sim 2 \text{ ns}$) and estimated diffusion length of $\sim 1.2 \mu\text{m}$ for carriers in the GaAs films on metal foils. Accordingly, we designed the base thickness (~ 0.8 – $1.2 \mu\text{m}$) to enable effective carrier collection.³⁰ However, the recombination at the grain boundaries, sidewalls and interfaces which are not completely understood may have contributed to the overall low EQE. The low EQE may also be due to inherent low-absorption coefficient of the GaAs films on metal substrates, indicated by separate optical studies not shown here. Further investigations are

underway to implement light management techniques (surface texture, back reflector) to enhance the optical absorption in the films. In overall, there remains a significant room for improvement to harness the full potential of the optoelectronic efficiency of these flexible GaAs solar cells. Improvement in defect density, introduction of passivation methods, incorporation of light-management techniques and development of multi-junction device design are essential and currently underway to further enhance the photo-conversion efficiency of these flexible GaAs devices on metal substrates.

4. Conclusions

We have demonstrated a method to produce epitaxial single-crystalline-like Ge films on metal foils using continuous roll-to-roll PECVD process. This marks a significant advancement towards scalable production of high-quality epi-Ge films on flexible, light-weight and inexpensive substrates for large-scale manufacturing of optoelectronic devices. The flexible CVD Ge films exhibited remarkable crystalline quality with strong biaxial texture and (001) orientation. The Ge templates were subsequently used for a proof-of-concept single-junction flexible GaAs device development. An 11.5% power conversion efficiency was achieved at 1 sun in the champion device, with V_{OC} of 642 ± 10 mV, J_{SC} of 25 ± 0.4 mA cm⁻², and FF of $72 \pm 2\%$, which is a record for GaAs solar cells directly deposited on alternative substrates. Improved quality GaAs films on CVD Ge templates resulted in increased efficiency. This work lays a pathway towards developing high-efficiency and low-cost GaAs solar cells on inexpensive flexible metal substrates. However, further improvement in defect density, grain-boundary passivation and device efficiency is required to propel this technology towards commercial success.

Conflicts of interest

There are no conflicts to declare.

Acknowledgements

This work is supported by funding from the U.S. Department of Energy (DOE) SunShot Initiative program (Award #: DE-EE-0006711), Advanced Manufacturing Institute, and Texas Center for Superconductivity at the University of Houston.

References

- 1 M. A. Green, Y. Hishikawa, E. D. Dunlop, D. H. Levi, J. Hohl-Ebinger Anita and W. Y. Ho-Baillie, Solar cell efficiency tables (version 51), *Prog. Photovoltaics*, 2018, **23**, 805–812.
- 2 E. Yablonovitch, T. Gmitter, J. P. Harbison and R. Bhat, Extreme selectivity in the lift-off of epitaxial GaAs films, *Appl. Phys. Lett.*, 1988, **51**, 2222.
- 3 M. Konagai, M. Sugimoto and K. Takahashi, High efficiency GaAs thin film solar cells by peeled film technology, *J. Cryst. Growth*, 1978, **45**, 277–280.
- 4 F. L. Wu, S. L. Ou, R. H. Horng and Y. C. Kao, Improvement in separation rate of epitaxial lift-off by hydrophilic solvent for GaAs solar cell applications, *Sol. Energy Mater. Sol. Cells*, 2014, **112**, 233–240.
- 5 S. Moon, K. Kim, Y. Kim, J. Heo and J. Lee, Highly efficient single-junction GaAs thin-film solar cell on flexible substrate, *Sci. Rep.*, 2016, **6**, 30107.
- 6 J. Yoon, S. Jo, I. S. Chun, I. Jung, H.-S. Kim, M. Meitl, E. Menard, X. Li, J. J. Coleman, U. Paik and J. A. Rogers, GaAs photovoltaics and optoelectronics using releasable multilayer epitaxial assemblies, *Nature*, 2010, **465**(7296), 329–333.
- 7 B. M. Kayes, H. Nie, R. Twist, S. G. Spruytte, F. Reinhardt, I. C. Kizilyalli and G. S. Higashi, 27.6% conversion efficiency, a new record for single-junction solar cells under 1 sun illumination, Proceedings of the 37th IEEE Photovoltaic Specialists Conference, 2011, pp. 4–8.
- 8 S. H. Kim, D.-M. Geum, M.-S. Park, C. Z. Kim and W. J. Choi, GaAs solar cell on Si substrate with good ohmic GaAs/Si interface by direct wafer bonding, *Sol. Energy Mater. Sol. Cells*, 2015, **141**, 372–376.
- 9 R. Fu, D. Feldman, R. Margolis, M. Woodhouse and K. Ardani, U.S. solar photovoltaic system cost benchmark, National Renewable Energy Laboratory, Golden, CO, USA, 2017, TP-6A20-68925.
- 10 M. Woodhouse and A. Goodrich, A manufacturing cost analysis relevant to single- and dual-junction photovoltaic cells fabricated with III-Vs and III-Vs grown on Czochralski silicon, National Renewable Energy Laboratory, Golden, CO, USA, 2013, PR-6A20-60126.
- 11 N. Jain and M. K. Hudait, III-V multijunction solar cell integration with silicon: present status, challenges and future outlook, *Energy Harvesting Syst.*, 2014, **1**, 121–145.
- 12 S. Essig, C. Allebe, T. Remo, J. F. Geisz, M. A. Steiner, K. Horowitz, L. Barraud, J. S. Ward, M. Schnabel, A. Descoeurdes, D. L. Young, M. Woodhouse, M. Despeisse, C. Ballif and A. Tamboli, Raising the One-Sun Conversion Efficiency of III-V/Si Solar Cells to 32.8% for Two Junctions and 35.9% for Three Junctions, *Nat. Energy*, 2017, **2**, 17144.
- 13 R. Cariou, J. Benick, P. Beutel, N. Razek, C. Flötgen, M. Hermle, D. Lackner, S. W. Glunz, A. W. Bett, M. Wimplinger and F. Dimroth, Monolithic Two-Terminal III-V/Si Triple Junction Solar Cells with 30.2% Efficiency Under 1-Sun AM1.5G, *IEEE J. Photovoltaics*, 2017, **7**, 367–373.
- 14 C. L. Andre, J. A. Carlin, J. J. Boeckl, D. M. Wilt, M. A. Smith, A. J. Pitera, M. L. Lee, E. A. Fitzgerald and S. A. Ringel, Investigations of high-performance GaAs solar cells grown on Ge-Si/sub 1-x/Ge/sub x/-Si substrates, *IEEE Trans. Electron Devices*, 2005, **52**(6), 1055–1060.
- 15 K. N. Yaung, M. Vaisman, J. Lang and M. L. Lee, GaAsP solar cells on GaP/Si with low threading dislocation density, *Appl. Phys. Lett.*, 2016, **109**(3), 032107.
- 16 S. A. Ringel, J. A. Carlin, C. L. Andre, M. K. Hudait, M. Gonzalez, D. M. Wilt, E. B. Clark, P. Jenkins, D. Scheiman, A. Allerman, E. A. Fitzgerald and C. W. Leitz, Single-junction InGaP/GaAs solar cells grown on Si substrates with SiGe buffer layers, *Prog. Photovoltaics*, 2002, **10**, 417.

- 17 Y. Wang, Z. Ren, M. Thway, K. Lee, S. F. Yoon, I. M. Peters, T. Buonassisi, E. A. Fitzgerald, C. S. Tan and K. H. Lee, Fabrication and characterization of single junction GaAs solar cells on Si with As-doped Ge buffer, *Sol. Energy Mater. Sol. Cells*, 2017, **172**, 140.
- 18 R. W. McClelland, C. O. Bozler and J. C. C. Fan, A technique for producing epitaxial films on reusable substrates, *Appl. Phys. Lett.*, 1980, **37**, 560–562.
- 19 M. Vaisman, N. Jain, Q. Li, K. M. Lau, A. C. Tamboli and E. L. Warren, *GaAs solar cells on V-grooved silicon via selective area growth*, in Proceedings 44th IEEE Photovoltaic Specialists Conference, 2017.
- 20 E. L. Warren, E. A. Makoutz, K. A. Horowitz, A. Dameron, A. G. Norman, P. Stradins, J. D. Zimmerman and A. C. Tamboli, *Selective area growth of GaAs on Si patterned using nanoimprint lithography*, Proceedings 43rd IEEE Photovoltaic Specialists Conference, 2016, pp. 1938–1941.
- 21 M. Vaisman, N. Jain, Q. Li, K. M. Lau, E. Makoutz, T. Saenz, W. E. McMahon, A. C. Tamboli and E. L. Warren, GaAs Solar Cells on Nanopatterned Si substrates, *IEEE J. Photovolt.* **3**, 2018, (4), 1635–1640.
- 22 R. Venkatasubramanian, B. C. O'Quinn, J. S. Hills, P. R. Sharps, M. L. Timmons, J. A. Hutchby, H. Field, A. Ahrenkiel and B. Keyes, *18.2% (AM1.5) efficient GaAs solar cell on optical grade polycrystalline Ge substrate*. Conference Record, 25th IEEE Photovoltaic Specialists Conference, Washington, 1997, pp. 31–36.
- 23 R. Venkatasubramanian, B. C. O'Quinn, E. Siivola, B. Keyes and R. Ahrenkiel, *20% (AM1.5) efficiency GaAs solar cells on sub-mm grainsize poly-Ge and its transition to low cost substrates*, Proceedings IEEE Photovoltaic Specialists Conference, 1997, vol. 811.
- 24 D. M. Wilt, M. A. Smith, W. Maurer, D. Scheiman and P. P. Jenkins, *GaAs Photovoltaics on Polycrystalline Ge Substrates*, IEEE 4th World Conference on Photovoltaic Energy Conference, Waikoloa, HI, USA, 2006, vol. 2, p. 1891.
- 25 S. J. Polly, C. R. Plourde, C. G. Bailey, C. Leitz, C. Vineis, M. P. Brindak, D. V. Forbes, J. S. McNatt, S. M. Hubbard and R. P. Raffaele, Thin film III–V solar cells on Mo foil, 34th IEEE Photovoltaic Specialists Conference, 2009, pp. 1377–1380.
- 26 S. R. Kurtz and R. McConnell, Requirements for a 20%-Efficient Polycrystalline GaAs Solar Cell, *AIP Conf. Proc.*, 1997, **404**, 191–205.
- 27 C. W. Teplin, D. S. Ginley and H. M. Branz, A new approach to thin film crystal silicon on glass: biaxially-textured silicon on foreign template layers, *J. Non-Cryst. Solids*, 2006, **352**, 984–988.
- 28 V. Selvamanickam, S. Sambandam, A. Sundaram, S. Lee, A. Rar, X. Xiong, A. Alemu, C. Boney and A. Freundlich, Germanium films with strong in-plane and out-of-plane texture on flexible, randomly textured metal substrates, *J. Cryst. Growth*, 2009, **311**, 4553.
- 29 J. R. Groves, J. B. Li, B. M. Clemens, V. LaSalvia, F. Hasoon, H. M. Branz and C. W. Teplin, Biaxially-textured photovoltaic film crystal silicon on ion beam assisted deposition CaF₂ seed layers on glass, *Energy Environ. Sci.*, 2012, **5**, 6905–6908.
- 30 C. Gaire, P. C. Clemmer, H.-F. Li, T. C. Parker, P. Snow, I. Bhat, S. Lee, G.-C. Wang and T.-M. Lu, Small angle grain boundary Ge films on biaxial CaF₂/glass substrate, *J. Cryst. Growth*, 2010, **312**, 607–610.
- 31 M. Asadirad, Y. Gao, P. Dutta, S. Shervin, S. Sun, S. Ravipati, S. H. Kim, Y. Yao, K. H. Lee, A. P. Litvinchuk, V. Selvamanickam and J.-H. Ryou, High-Performance Flexible Thin-Film Transistors Based on Single-Crystal-Like Germanium on Glass, *Adv. Electron. Mater.*, 2016, **2**, 1600041.
- 32 R. Wang, S. N. Sambandam, G. Majkic, E. Galstyan and V. Selvamanickam, High mobility single-crystalline-like germanium thin films on flexible, inexpensive substrates, *Thin Solid Films*, 2013, **9**, 527–532.
- 33 P. Dutta, Y. Gao, M. Rathi, Y. Yao, M. Iliev, J. Martinez and V. Selvamanickam, High mobility single-crystalline-like silicon thin films on inexpensive flexible metal foils by plasma enhanced chemical vapor deposition, *Acta Mater.*, 2018, **147C**, 51–58.
- 34 C. W. Teplin, M. P. Paranthaman, T. R. Fanning, K. Alberi, L. Heatherly, S. H. Wee, K. Kim, F. A. List, J. Pineau, J. Bornstein, K. Bowers, D. F. Lee, C. Cantoni, S. Hane, P. Schroeter, D. L. Young, E. Iwaniczko, K. M. Jones and H. M. Branz, Heteroepitaxial film crystal silicon on Al₂O₃: new route to inexpensive crystal silicon photovoltaics, *Energy Environ. Sci.*, 2011, **4**, 3346.
- 35 V. Selvamanickam, H.-G. Lee, Y. Li, J. Reeves, Y. Qiao, Y. Y. Xie, K. Lenseth, G. Carota, M. Funk, K. Zdun, J. Xie, K. Likes, M. Jones, L. Hope and D. W. Hazelton, Scale up of high-performance Y–Ba–Cu–O coated conductors, *IEEE Trans. Appl. Supercond.*, 2003, **13**, 2492–2495.
- 36 P. N. Arendt and S. R. Foltyn, Biaxially Textured IBAD-MgO Templates for YBCO-Coated Conductors, *MRS Bull.*, 2004, **29**, 543.
- 37 P. Dutta, M. Rathi, Y. Yao, Y. Gao, G. Majkic, M. Iliev, J. Martinez, B. Holzapfel and V. Selvamanickam, Large grained single-crystalline-like germanium thin film on flexible NiW tape, *RSC Adv.*, 2014, **4**, 21042.
- 38 M. Rathi, P. Dutta, N. Zheng, Y. Yao, D. Khatiwada, Y. Gao, S. Sun, Y. Li, S. Pouladi, P. Ahrenkiel, J.-H. Ryou and V. Selvamanickam, High opto-electronic quality n-type single-crystalline-like GaAs thin films on flexible metal substrates, *J. Mater. Chem. C*, 2017, **5**, 7919–7926.
- 39 P. Dutta, M. Rathi, N. Zheng, Y. Gao, Y. Yao, J. Martinez, P. Ahrenkiel and V. Selvamanickam, High mobility single-crystalline-like GaAs thin films on flexible, inexpensive substrates, *Appl. Phys. Lett.*, 2014, **105**, 092104.
- 40 V. Selvamanickam, S. Sambandam, A. Sundaram, S. Lee, A. Rar, X. Xiong, A. Alemu, C. Boney and A. Freundlich, Germanium films with strong in-plane and out-of-plane texture on flexible, randomly textured metal substrates, *J. Cryst. Growth*, 2009, **311**, 4553.
- 41 M. Rathi, P. Dutta, N. Zheng, Y. Yao, Y. Gao, S. Sun, A. Khadimallah, M. Thomas, M. Asadirad, P. Ahrenkiel, J. Ryou and V. Selvamanickam, *AlGaAs/GaAs DH and InGaP/GaAs DH grown by MOCVD on flexible metal substrates*, IEEE 43rd Photovoltaic Specialists Conference (PVSC), 2016, pp. 1926–1928.

- 42 P. Dutta, M. Rathi, P. Ahrenkiel, Y. Gao, A. Mehrotra, E. Galstyan, M. Iliev, B. Makarenko, R. Forrest, A. Freundlich and V. Selvamanickam, *Epitaxial thin film GaAs deposited by MOCVD on Low-Cost, Flexible Substrates for High Efficiency Photovoltaics*, IEEE 39th Photovoltaic Specialists Conference (PVSC), 2013, pp. 3393–3396.
- 43 G. Venugopal Rao, G. Amarendra, B. Viswanathan, S. Kanakaraju, S. Balaji, S. Mohan and A. K. Sood, Studies on Ge/CeO₂ thin film system using positron beam and Raman spectroscopy, *Thin Solid Films*, 2002, **406**, 250–254.
- 44 C.-Y. Tsao, J. W. Weber, P. Campbell, P. I. Widenborg, D. Song and M. A. Green, Low-temperature growth of polycrystalline Ge thin film on glass by *in situ* deposition and ex situ solid-phase crystallization for photovoltaic applications, *Appl. Surf. Sci.*, 2009, **255**, 7028–7035.
- 45 O. Breitenstein, J. Bauer, A. Lotnyk and J.-M. Wagner, Defect induced non-ideal dark IV characteristics of solar cells, *Superlattices Microstruct.*, 2009, **45**, 182189.
- 46 D. Khatiwada, P. Dutta, M. Rathi, B. Yu, C. Favela, Y. Yao, S. Sun, Y. Li, S. Pouladi and J.-H. Ryou, V. Selvamanickam, *Impact of Passivation on Base Thickness for Single Junction Flexible GaAs Solar Cells on Epi-ready Metal Tape*, Proceedings of 2018 IEEE 7th World Conference on Photovoltaic Energy Conversion (WCPEC), 2018, pp. 1822–1825.
- 47 P. Dutta, J. Poplawsky, H. Guthrey, M. Rathi, D. Khatiwada, S. Sun, Y. Yao, B. Yu, E. Galstyan and V. Selvamanickam, *Nanoscale investigation of grain boundary characteristics of single-crystalline-like GaAs films and solar cells on flexible metal substrates*, Proceedings of 2018 IEEE 7th World Conference on Photovoltaic Energy Conversion (WCPEC), 2018, pp. 58–61.
- 48 N. Jain and M. Hudait, Impact of Threading Dislocations on the Design of GaAs and InGaP/GaAs Solar Cells on Si Using Finite Element Analysis, *IEEE J. Photovoltaics*, 2013, **3**, 528–534.

Electronic Supplemental Information for:

Flexible GaAs solar cells on roll-to-roll processed epitaxial Ge films on metal foils: a route towards low-cost and high-performance III-V photovoltaics

P. Dutta^{1,2,3}, M. Rathi^{1,2,3}, D. Khatiwada^{1,2,3}, S. Sun^{1,2,3}, Y. Yao^{1,2,3}, B. Yu^{1,2,3}, S. Reed¹, M. Kacharia⁶, J. Martinez⁴, A. Litvinchuk³, Z. Pasala⁵, S. Pouladi¹, B. Eslami¹, J. -H. Ryou^{1,2,3}, H. Ghasemi¹, P. Ahrenkiel⁵, S. Hubbard⁶, V. Selvamanickam^{1,2,3}

¹ Department of Mechanical Engineering, University of Houston, Houston, TX 77204, USA

² Advanced Manufacturing Institute, University of Houston, Houston, TX 77204, USA

³ Texas Center for Superconductivity, University of Houston, Houston, TX 77204, USA

⁴ Materials Evaluation Laboratory, NASA Johnson Space Center, Houston, TX 77085, USA

⁵ Nanoscience and Nanoengineering, South Dakota School of Mines and Technology, Rapid City, SD 57701, USA

⁶ Department of Physics & Microsystems Engineering, Rochester Institute of Technology, Rochester, NY 14623

Description of R2R PECVD for Ge growth

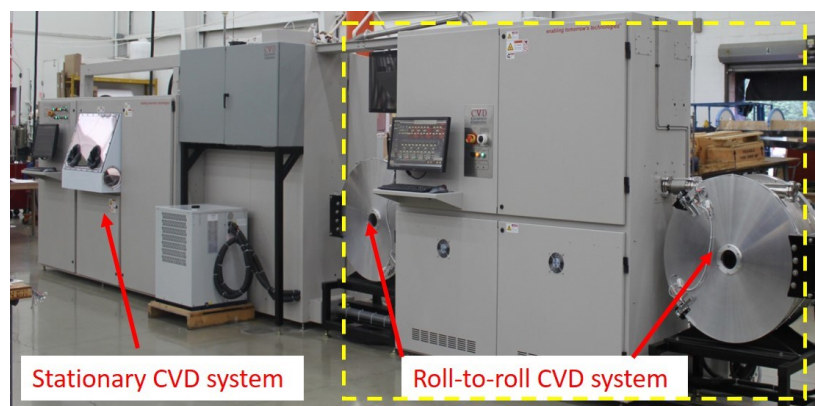


Figure S1. R2R CVD system custom-designed and developed at U of H to deposit the Ge films continuously on moving metallic foils. The blue arrows show the dispense and take-up spools.

The custom-designed roll-to-roll R2R-CVD tool for scalable processing of Ge films on moving metallic tapes is shown in figure S1. The spools with substrates are loaded in the cylindrical spool chambers which can hold over a kilometer length of substrates. The tool is designed for multi-pass capability to coat multiple layers needed for device structures, by passing

the tape back and forth in the reactor between the spool chambers. A polymeric interleaf film is used to protect the deposited films from contamination. The R2R system is also capable for growth of III-V materials by metal organic chemical vapor deposition. The typical stationary CVD chamber is shown on the left, where all the standard optimization runs are carried out before moving on to the long-length R2R processes.

Dark current vs voltage plots of GaAs PV on sputter and CVD Ge substrate

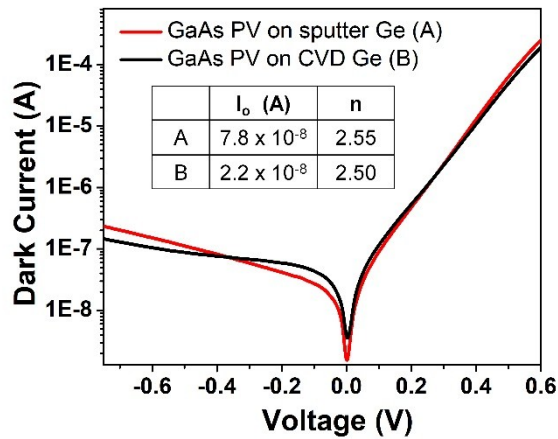


Figure S2. Dark I-V plots of flexible GaAs solar cells on CVD Ge and sputtered Ge template on metal foil substrates.

Figure S2 shows the dark current-voltage (I-V) plots of the GaAs solar cells fabricated on CVD and sputtered Ge templates. The reverse saturation currents (I_0) were 2.2 and 7.8×10^{-8} A and ideality factors 2.5 and 2.55 for GaAs p-n diodes on CVD and sputtered templates, respectively. The I-V curve was fitted with the diode equation $I = I_0(e^{eV/nKT} - 1)$ to determine the saturation current (I_0) and ideality factors (n), where

I = current across the diode

I_0 = reverse saturation current

V = applied voltage

e = electron charge

k = Boltzmann constant

T = temperature

Illuminated current vs voltage of GaAs PV on CVD Ge substrate

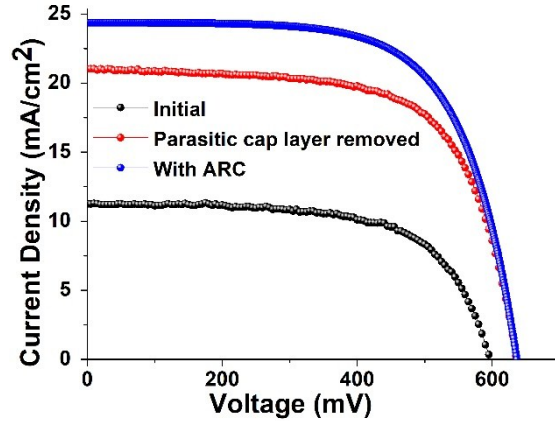


Figure S3. *J-V plots of GaAs SJ solar cell on CVD Ge on metal substrate showing the improvement in device properties with parasitic layer removal and ARC coating*

Table T1: Device parameters of GaAs solar cell on metal substrate

	V_{oc} (V)	J_{sc} (mA/cm ²)	FF (%)	Efficiency (%)
Initial	592	11.4	67	4.3
Parasitic cap layer removed	634	21.0	69	8.8
With ARC	642	23.5	72	10.5
With shadowing adjustment	642	25.0	72	11.5

Figure S3 shows the illuminated J-V plots of a representative GaAs SJ solar cell on metal substrate measured at three stages of device fabrication, as fabricated, parasitic cap layer removed and with final ARC layer. The table T1 shows the device parameters extracted from the J-V plots. The V_{oc} increased from 592 to 642 (50 mV increase) and the J_{sc} increased significantly from 11.4 to 23.5 mA/cm², resulting in an increase of device efficiency from 4.3 to 10.5 %. The increase of V_{oc} and J_{sc} can be attributed to the passivation of side walls (reduction of

recombination) and increased light absorption due to the removal of the parasitic cap layer (30 nm GaAs highly doped layer) and incorporation of ARC coating. The device efficiency increased further when the shadowing effect is taken into consideration and the effective device area was adjusted.

Table T2: Device data of GaAs solar cells on CVD and sputtered Ge template showing results of 3 devices.

GaAs device on CVD Ge template					GaAs device on sputtered Ge template				
Device #	Eff (%)	Voc (mV)	Jsc (mA/cm ²)	FF (%)	Device #	Eff (%)	Voc (mV)	Jsc (mA/cm ²)	FF (%)
CVD1	11.5	642	25	72	Sput1	6.7	570	18.6	63
CVD2	8.8	606	19	70	Sput2	5.2	531	15	65
CVD3	6.8	622	18.2	64	Sput3	6.4	571	16.5	66
CVD4	8.1	612	18.5	72	Sput4	6.5	550	17.1	69

Table 1 shows the results of four GaAs devices on CVD and sputtered Ge templates. The first row shows the champion device, as reported in the manuscript. The next two rows show two other devices made during the same period of same size (500 μm dia).

Table T3: Representative device data of GaAs solar cells on sputtered Ge template showing results of 4 different device sizes.

Device ID	Dia (μm)	Voc (mV)	Jsc (mA/cm ²)	FF (%)	Eff (%)
A	500	549	16.8	72	6.6
B	750	543	15.8	64	5.5
C	1000	542	15	65	5
D	1250	534	15.4	62	5.1

Table T3 shows the effect of device size on the performance of devices on sputtered Ge template. It was observed that with the increase in device size, there was a drop in performance. Here, a decrease in device efficiency from 6.6 % to 5.1 % was observed as the device size increased from 500 to 1250 μm . This trend was observed in general for all devices made on CVD and sputtered Ge templates on IBAD textured metal foils.

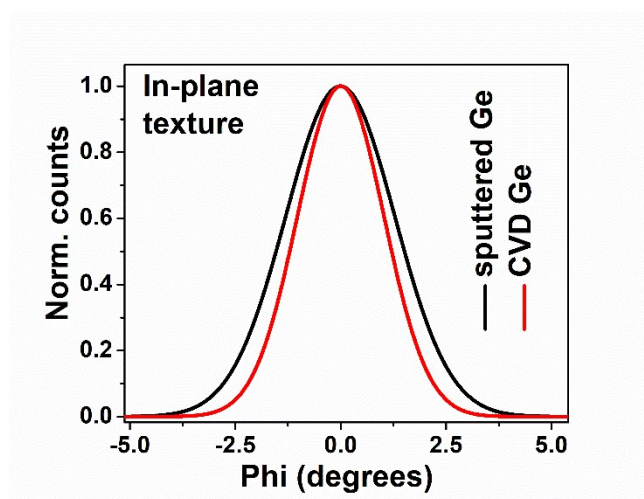


Figure S4. *In-plane phi-scan showing the narrowing of FWHM in CVD Ge film compared to sputtered film indicating improvement in crystalline alignment in CVD Ge films*

The crystalline alignment of CVD Ge in the in-plane direction showed improvement compared to sputtered Ge. Figure S4 shows the normalized counts vs Phi angle plot of CVD and sputtered Ge film. The in-plane texture (peak width or FWHM) were 2.4 and 3 degrees for CVD and sputtered Ge respectively. Decrease in peak width of CVD Ge was observed which indicated enhancement in crystalline alignment in CVD Ge films.